

Propagation of Alfvén waves in the charge starvation regime

Pawan Kumar¹★, Ramandeep Gill^{2,3}†, Wenbin Lu^{4,5}‡

¹*Department of Astronomy, University of Texas at Austin, Austin, TX 78712, USA*

²*Instituto de Radioastronomía y Astrofísica, Universidad Nacional Autónoma de México, Antigua Carretera a Pátzcuaro # 8701, Ex-Hda. San José de la Huerta, Morelia, Michoacán, México C.P. 58089*

³*Astrophysics Research Center of the Open University (ARCO), The Open University of Israel, P.O Box 808, Ra'anana 4353701, Israel*

⁴*Departments of Astronomy and Theoretical Astrophysics Center, UC Berkeley, Berkeley, CA 94720, USA*

⁵*Department of Astrophysical Sciences, Princeton University, Princeton, NJ 08544, USA*

29 August 2022

ABSTRACT

We present numerical simulation results for the propagation of Alfvén waves in the charge starvation regime. This is the regime where the plasma density is below the critical value required to supply the current for the wave. We analyze a conservative scenario where Alfvén waves pick up charges from the region where the charge density exceeds the critical value and advect them along at a high Lorentz factor. The system consisting of the Alfvén wave and charges being carried with it, which we call charge-carrying Alfvén wave (CC-AW), moves through a medium with small, but non-zero, plasma density. We find that the interaction between CC-AW and the stationary medium has a 2-stream like instability which leads to the emergence of a strong electric field along the direction of the unperturbed magnetic field. The growth rate of this instability is of order the plasma frequency of the medium encountered by the CC-AW. Our numerical code follows the system for hundreds of wave periods. The numerical calculations suggest that the final strength of the electric field is of order a few percent of the Alfvén wave amplitude. Little radiation is produced by the sinusoidally oscillating currents associated with the instability during the linear growth phase. However, in the nonlinear phase, the fluctuating current density produces strong EM radiation near the plasma frequency and limits the growth of the instability.

Key words: fast radio bursts – stars: neutron – radio continuum: transients

1 INTRODUCTION

Finite amplitude magnetic field disturbances, or Alfvén waves, are ubiquitous in astrophysical plasma. They are found in the interstellar medium, stellar atmospheres, accretion disks, the magnetosphere of neutron stars, etc. There is a non-zero current density along the direction of the unperturbed magnetic field (\mathbf{B}_0) when the wave-vector of an Alfvén wave is not exactly aligned with \mathbf{B}_0 . If the wave propagates in a medium of decreasing plasma density, under some generic conditions, it might face the situation where it enters a region with too little density to be able to supply the current for the Alfvén wave even when charged particles move at the speed of light, i.e. $|\hat{\mathbf{B}}_0 \cdot \nabla \times \mathbf{B}| > 4\pi qn$, where $\hat{\mathbf{B}}_0$ is a unit vector along \mathbf{B}_0 , n is the total charge density of electrons and positrons and q is the elementary charge.

The Alfvén wave is said to have entered the charge starvation region in this case or that the wave has become charge starved. We are interested in understanding what happens to the Alfvén wave and its interaction with particles it encounters in this condition. The

application we have in mind is the magnetosphere of a neutron star where some disturbance in the interior of the star propagates to the surface and shakes up the magnetosphere. Numerous papers have suggested that some fraction of the Alfvén wave energy when it enters the charge starvation regime is converted to coherent radio emission, e.g. Kumar et al. (2017); Lu & Kumar (2018); Yang & Zhang (2018); Ioka & Zhang (2020); Zhang (2020); Kumar & Bošnjak (2020); Lu et al. (2020); Cooper & Wijers (2021); Wang et al. (2021); Qu & Zhang (2021). The generation of coherent radiation requires that strong electric fields develop along \mathbf{B}_0 in the charge starvation regime. There are also claims to the contrary, e.g. Chen et al. (2020), that nothing interesting happens to the Alfvén wave when it becomes charge starved. These papers suggest that the wave simply advects charge particles with it when it enters the charge starvation region so that it is never truly charge starved, and that a strong electric field along \mathbf{B}_0 never develops to accelerate charge particles to highly relativistic speeds and generate coherent radiation.

In Section 2, we consider propagation of charge-carrying Alfvén waves (CC-AW) in vacuum and show that even in this case, an electric field parallel to the static magnetic field slowly develops over time.

In Section 3, we consider CC-AW propagating into a low density stationary plasma, and in this case we find that the interaction leads

★ pk@astro.as.utexas.edu

† r.gill@irya.unam.mx

‡ wenbinlu@berkeley.edu

to rapid growth of an electric field which accelerates charge particles and leads to the dissipation of the Alfvén wave (AW).

2 ADVECTION OF CHARGE PARTICLES BY ALFVÉN WAVES AT THE THRESHOLD OF CHARGE STARVATION

We investigate the scenario where an Alfvén wave (AW) packet advects charge particles with it so that it is initially not charge starved. The unperturbed magnetic field is taken to be homogeneous and pointing along the z -axis. Perturbation to the magnetic field and the \hat{z} -component of the current density are described by

$$\mathbf{B}_y = \hat{\mathbf{y}}B_y \exp(i\psi),$$

$$j_0 = \frac{c}{4\pi} (\nabla \times \mathbf{B}_y)_z = \frac{ick_x B_y}{4\pi} \exp(i\psi), \quad (1)$$

where $\psi \equiv k_x x + k_z z - \omega_a t$, and ω_a is the Alfvén wave frequency. The particular scenario we are considering is where the AW carries charge particles with sufficient density to supply the current j_0 in equation (1). These particles are taken to move with Lorentz factor (LF) γ_0 that is independent of z initially. In this case, the particle number density is given by

$$n(t, z) = \frac{j_0}{qc} = \frac{ik_x B_y}{4\pi q} \exp(i\psi), \quad (2)$$

where q is the charge of e^\pm advected by the AW. Strictly speaking, the charge density also depends on x through the dependence of ψ on x , however, it does so over much larger length scales $\sim k_x^{-1}$, and so this dependence is ignored here. According to this solution, half of the wave-packet advects positrons with it and the adjoining half advects electrons as shown in Fig. 1. These solutions satisfy the particle flux continuity equation and Maxwell's equations.

The particle flux equation

$$\frac{\partial n}{\partial t} + \frac{\partial v_z n}{\partial z} = 0, \quad (3)$$

is 1D because particles are confined to move along the magnetic field lines; for high particle LF $v_z \approx c$. The particle density (eq. 2) satisfies the continuity equation, as $ck_z = \omega_a$ is the dispersion relation for the Alfvén wave. The x -component of Ampere's law (Maxwell equation for $\nabla \times \mathbf{B}$) gives $E_x = B_y$; plasma current along \hat{x} is zero as charge particles can only move along the magnetic field. The y -component of the Induction equation

$$\frac{\partial E_x}{\partial z} - \frac{\partial E_z}{\partial x} = i\omega_a B_y / c \quad \text{or} \quad k_z E_x = \omega_a B_y / c \quad (4)$$

is satisfied as can be seen from the AW dispersion relation. The other two components of the induction equations are satisfied identically. Thus, the solution given by eqs. (1) & (2) satisfies particle flux and Maxwell equations to $O(B_y)$. This solution has the property that charge particles of opposite signs are completely separated spatially with positrons in the region with positive $[\nabla \times \mathbf{B}_y]_z$ and electrons where this curl is negative. These charge particles move along the magnetic field at high Lorentz factor and provide the current-density the AW needs along \hat{z} .

The Coulomb field along the unperturbed magnetic field due to the charge separation is best calculated in the rest frame of the charges

and is given by¹

$$E_{z,\text{coulomb}} \sim \frac{2\pi q n}{\gamma_0} \frac{d \ln n}{dz} \left(\frac{r}{\gamma_0} \right)^2 \sim \frac{2\pi j_0 k_z r^2}{c \gamma_0^3}, \quad (5)$$

where r is the distance the wave has traveled from its launching site. This is a very weak field for large γ_0 and it is superseded by the field that arises due to the current deficit that develops with time; the current deficit develops because charge particles lag the AW slightly, even when γ_0 is large, and this lag increases with time.

It should be pointed out that acceleration of particles to high LFs might pose a problem since the Coulomb field is strong for small γ_0 and the electric field direction switches as the sign of the charge density gradient changes. Thus, only half the particles of one sign are accelerated and the other half are decelerated by this field. The only way out of this problem might be that particles are accelerated to high LF while the plasma is almost neutral, which is not the condition conducive to strong electric field and particle acceleration. So, the viability of this scenario – charges advected by Alfvén wave at high LF to supply the current the wave requires – is uncertain. Nevertheless, we assume that such a set up is physically plausible, and proceed to investigate whether this solution is stable and how it evolves with time. Our goal is to determine whether an AW packet will advect particles to avoid charge-starvation and hence energy dissipation. We show that even in the conservative scenario where particles are perfectly advected initially, the CC-AW strongly interacts with the plasma ahead of it causing the dissipation of the AW and generation of coherent radio emission.

2.1 Development of current deficit and emergence of electric field: the vacuum case

Let us consider a fully ionized plasma where charges of opposite signs are completely separate spatially, and the particle density is $n(z)$. The current when particles are moving with Lorentz factor (LF) γ_0 or speed v_0 is j . The maximum current that this plasma can supply is

$$j_{\text{max}} = \frac{jc}{v_0} \approx j \left(1 + \frac{1}{2\gamma_0^2} \right), \quad (6)$$

where $c/v_0 = \beta_0^{-1} = (1 - \gamma_0^{-2})^{-1/2} \approx (1 + 1/2\gamma_0^2)$ for $\gamma_0 \gg 1$. If the current deficit, $\delta j \equiv j_0 - j$, were to exceed $j/2\gamma_0^2$ then no amount of acceleration of plasma can make up for this current deficit as long as the plasma density does not increase (j_0 is given by eq. 1). If plasma density were to increase at one location then that can be only at the expense of lower density at another location, thereby making current deficit larger at this other location.

Let us start with zero current deficit everywhere, i.e. $\delta j(z, t = 0) = 0$. The current deficit develops with time in some regions of the AW due to the fact that particle speed is always less than the speed of Alfvén waves. AW speed is given by: $v_A/c = 1 - \omega_p^2/2\omega_B^2$ (Krall & Trivelpiece 1973; Kulsrud 2005), and the corresponding LF is $\gamma_A \sim \omega_B/\omega_p \gg 10^6$ in NS magnetosphere; where $\omega_p = (4\pi n q^2/m)^{1/2}$ is the plasma frequency, and $\omega_B = qB_0/mc$ is the cyclotron frequency.

¹ The various factors in the expression for the Coulomb field are as follows. The charge density in the charge comoving frame is n/γ_0 . The width of the causally connected slab in the comoving frame is $\sim r/\gamma_0$, and $d \ln n/dz(r/\gamma_0)$ gives the charge density difference in the two-halves of the causally connected region; the electric field vanishes when the charge is uniformly distributed.

The slip that develops between particles and the AW in time T is $\delta z = Tc/2\gamma_0^2$, and thus $\delta j \approx \delta z(dj_0/dz)$, or

$$\delta j \approx \text{sign} \left(\frac{dj_0}{dz} \right) \frac{j_0}{2\gamma_0^2} \left(\frac{Tc}{\lambda_a} \right), \quad (7)$$

where λ_a is AW wavelength along z . This equation tells us that the current deficit increases linearly with time, due to the finite particle speed, and in one wave period the deficit becomes too large to be eliminated entirely no matter how rapidly particles are accelerated. The z -component of the electric field that develops due to this current deficit or surplus is

$$E_z(z, t) = -4\pi \int dt \delta j. \quad (8)$$

Or

$$E_z = 2\pi Tc \int \frac{dz}{c} \frac{1}{\gamma_0^2} \frac{dj_0}{dz} \approx \frac{2\pi T}{\gamma_0^2} [j_0(z, t)] \quad (9)$$

where we took γ_0 to be independent of z , and the last equality is obtained by integrating over half a wavelength of the AW to obtain the peak amplitude of E_z . Comparing this E_z with the Coulomb field (eq. 5), we see that the electric field that develops due to current deficit is larger by a factor $\gamma_0/(rk_z)$. We can rewrite E_z in terms of the magnetic field perturbation associated with the AW by making use of the expression for j_0 (eq. 1)

$$E_z \sim \frac{B_y(\omega_a T)}{2\gamma_0^2} \left(\frac{k_x}{k_z} \right) \quad (10)$$

The LF of e^\pm changes in time T due to this electric field by an amount

$$\delta\gamma_0 \sim \frac{qE_z c T}{mc^2} \sim \frac{qB_y}{mc} \left[\frac{(\omega_a T)T}{2\gamma_0^2} \right] \left(\frac{k_x}{k_z} \right) \quad (11)$$

This suggests that particles might attain an asymptotic LF of

$$\gamma_0 \rightarrow \left[\frac{(qB_y)\omega_a T^2 k_x}{2mck_z} \right]^{1/3}. \quad (12)$$

However, it should be pointed out that the electric field in one-quarter of the wavelength where the gradient of j_0 is positive will develop negative electric field, and in the adjoining quarter wavelength the field would be along positive z . Therefore, e^\pm s in the former case would be decelerated while in the latter case accelerated. This velocity different would grow quadratically with time, and the simple AW solution described by equation (1) will not hold for very long.

Moreover, what we have described in this section is a highly idealized situation where the charge carrying AW (CC-AW) is propagating through a medium with zero plasma density; from here on we shall use the compact name **CC-AW** for the system consisting of an Alfvén wave plus the particles being advected with it at high speeds. A physically more realistic situation is that the CC-AW encounters a nearly stationary plasma of low density as it travels further out into the magnetosphere. The interactions between the Alfvén wave, the charge particles it is advecting along at high speeds, and the stationary plasma they encounter, make this system complex and full of interesting physics. The consequences of these interactions for the development of the z -component of the electric field, and the evolution and dissipation of AWs are topics that we explore in the next two sections.

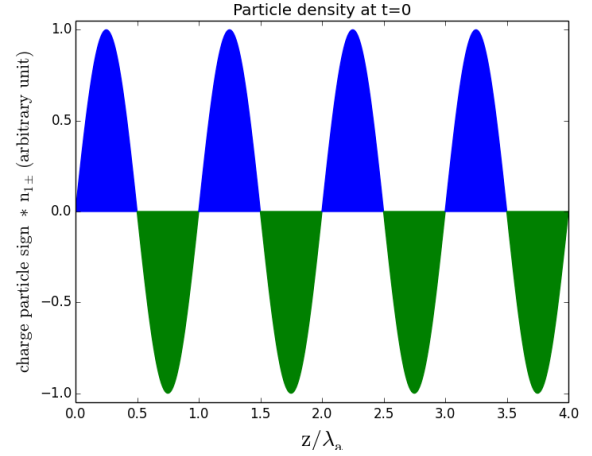


Figure 1. Shown here is the initial density, at $t = 0$, of e^\pm times the sign of the charge particle advected by the Alfvén wave as a function of the z -coordinate which is the direction of propagation of the wave; $n_{1\pm}$ is given by eq. 17, $\lambda_a \equiv 2\pi c/\omega_a$ is AW wavelength along the z -direction. Note that positron density is shown here as positive numbers and electron density as negative numbers. The charges are fully separated initially, as the different color shadings indicate, and they are all moving at the same speed v_0 corresponding to Lorentz factor 10^2 initially. The current density at $t = 0$ is precisely equal to $c(\nabla \times \mathbf{B})_z/4\pi$ as given by equation 17.

3 INTERACTION BETWEEN CHARGE CARRYING ALFVÉN WAVE (CC-AW) AND STATIONARY PLASMA

We consider the physics of an Alfvén wave packet that is advecting charge particles with it, and they encounter stationary electron-positron plasma of low density that is charge neutral. We shall consider a set of 2D equations (one space dimension and time), which is faster to solve numerically. The CC-AW is taken to propagate along the z -axis. The x -dependence of all variables is $\exp(ik_x x)$, and they are all independent of y . The conservation of magnetic flux together with $k_y = 0$, $k_x \neq 0$, and $k_z \neq 0$ ensures that only the \hat{y} component of the magnetic field perturbation, B_y , is non-zero. Thus, the non-zero components of the Maxwell's equations are

$$-\partial_z B_y = \partial_t E_x/c, \quad ik_x B_y = 4\pi j_z/c + \partial_t E_z/c \quad (13)$$

$$\partial_z E_x - ik_x E_z = -\partial_t B_y/c \quad (14)$$

These combined with the following particle continuity and momentum flux conservation equations provide a complete description of the 2D problem,

$$\partial_t n + \partial_z(nv_z) = 0 \quad \& \quad \partial_t(\gamma v_z) + v_z \partial_z(\gamma v_z) = \frac{qE_z}{m} \quad (15)$$

$$\text{or} \quad \partial_t(v_z) + v_z \partial_z(v_z) = \frac{qE_z}{m\gamma^3}. \quad (16)$$

We consider only the z -component of the momentum equation as particles are locked in the lowest Landau state in the presence of the strong magnetic field being considered in this work, and hence confined to move along the magnetic field.

The initial conditions we use are²,

$$\begin{aligned}
 B_y(t=0, z) &= \epsilon B_0 \sin(\omega_a z/c), \quad \text{for } 0 < z < z_0 \\
 E_x(t=0, z) &= \epsilon B_0 \sin(\omega_a z/c), \quad E_z(t=0, z) = 0, \\
 E_z(t, z=tc) &= 0, \quad j_{z1}(t=0, z) = c [\nabla \times \mathbf{B}_y]_z / 4\pi \\
 v_{1z}(t=0, z) &= v_0 \equiv (1 - \gamma_0^{-2})^{1/2} \\
 n_1(t=0, z) &= j_z / [qv_0 \text{sign}(j_z)],
 \end{aligned} \tag{17}$$

where B_0 is the unperturbed magnetic field strength, ϵ and ω_a are the AW amplitude (dimensionless) and frequency respectively, and the AW initially has only positrons in the part of the wave packet where the current density is positive, i.e. $j_z > 0$, and electrons where $j_z < 0$. All particles advected by the wave are taken to have speed v_0 initially. The initial particle density distribution along z -axis is shown in Fig. (1).

The boundary condition at the head of the AW is that stationary plasma, that is charge neutral, with prescribed constant density n_2 enters the wave, and E_z is the Coulomb field of the CC-AW. The boundary condition at the rear end of the AW is that no particles enter the system here.

For convenience of later use we define a frequency associated with the particle density advected with the AW

$$\omega_{p1}(z) \equiv \left[\frac{4\pi q^2 n_1(z)}{m} \right]^{1/2}, \tag{18}$$

which is not the physical plasma frequency as it is missing a factor of γ_0 ; we will include the correct factor when using ω_{p1} to construct the plasma frequency.

The CC-AW – AW along with particles with density $n_1(z)$ advected by the wave – encounters stationary e^\pm plasma of density n_2 as they travel outward to larger z . In all of our simulations we take n_2 to be independent of t and z before particles are accelerated by the CC-AW. And we experiment with a number of different values of $n_2/\max[n_1(z)] < 1$ in our numerical simulations.

We consider in the next sub-section an approximation where the fields $B_y(t, x, z)$ and $E_x(t, x, z)$ are specified, i.e. these components of the fields are pre-set to be the time translation of the function in equation (17). This simplification makes it possible to easily understand, using analytical methods, some of the key features of our numerical simulation results. Numerical solutions of the exact problem, without these approximations, are presented in §3.2 where we show that the main features of the solutions are essentially the same as obtained with the aforementioned approximations.

² The initial conditions for the numerical analysis presented in this work (eq. 17) is motivated in part by the PIC simulations carried out by [Chen et al. \(2020\)](#) of Alfvén wave propagation in a stratified medium where the particle density for the first few wavelengths is sufficiently high (so that the waves are not charge starved) and then the wave enters a medium with density much smaller than the critical density for the AW. They find the development of charge separation, and acceleration of particles to Lorentz factors of a few 10s when the wave enters the low density medium. Thus, according to their simulations, the AW carries charge particles with it into vacuum thereby preventing the charge starvation. The viability and stability of this scenario when the wave travels a distance of 10^2 s of wavelength is investigated in this work.

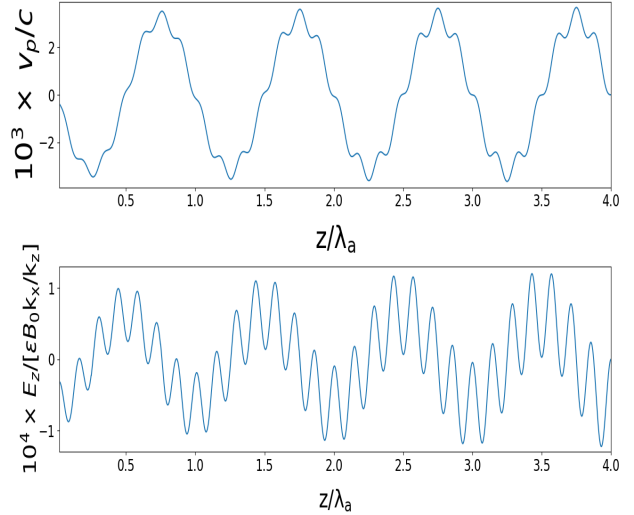


Figure 2. Stationary e^\pm encountered by charge-carrying-AW-packet (shown in Fig. 1) get accelerated by the z -component of the electric field (E_z) shown in the lower panel. The upper panel shows the speed of e^\pm s, at a fixed time, along the extent of AW packet on the z -axis (ct should be added to the z -coordinate shown in the figure to obtain the lab frame location of the AW); the unperturbed magnetic field is along z , $\epsilon = 10^{-3}$, and ϵB_0 is the amplitude of the Alfvén wave packet. The positron speed and E_z were calculated at $t = 10T_a$ by numerically solving eqs. 13–16 with the simplifying assumption that B_y is given by equation 19; $T_a = 2\pi/\omega_a$ & $\lambda_a = cT_a$ are the Alfvén wave period and wavelength respectively. We took $\gamma_0 = 10^2$, $k_x/k_z = 0.5$, $\omega_B/\omega_a = qB_0/(mc\omega_a) = 10^5$, the plasma frequency of the stationary e^\pm plasma, ω_{p2} , is 7.1 times the Alfvén wave frequency ω_a , and the peak value of ω_{p1} (defined by eq. 18) is 7.1 ω_a for these simulations.

3.1 Charge starved Alfvén wave propagation when the magnetic field perturbation is pre-specified

We assume in this sub-section that the magnetic field perturbation associated with the Alfvén wave packet shifts with time to larger z at speed c without any distortion to its amplitude or phase. This is not strictly correct. However, this assumption simplifies the calculation as the only EM field variable we need to evolve in this case is E_z ; the other two field components, viz. B_y and E_x , are known as per this assumption from the initial condition for the Alfvén wave packet. This assumption makes it possible to obtain approximate analytic solutions for the dynamics of the CC-AW system in the charge starvation regime and obtain physical insights regarding some of its basic properties. The magnetic field perturbation, B_y , according to this assumption, is explicitly given by:

$$B_y(t, x, z) = \epsilon B_0 \sin\left(\frac{\omega_a z}{c} + k_x x - \omega_a t\right), \tag{19}$$

where we have also assumed that the Lorentz factor of the Alfvén wave is much larger than the LF of particles, and thus taking the AW dispersion relation to be $\omega_a = k_z c$ is quite accurate.

We show in Figs. 2 & 3 numerical solutions of equations 13–16, with the approximation mentioned at the beginning of this subsection, for one set of parameters. We can understand the magnitude and the general behavior of the z -component of the electric field, E_z , that develops in this interaction using the following approximate calculation.

Let us write the current density as the sum of two parts. The first piece, j_{z1} is due to e^\pm advected by the AW, and the second component, j_{z2} , is due to the charge particles encountered by the CC-AW, which are accelerated along the \hat{z} direction due to non-

zero E_z . Rewriting Ampère's law with these two components of the current density separately we find

$$(\nabla \times \mathbf{B}_y)_z - \frac{4\pi j_{z1}}{c} \equiv -\frac{4\pi j'}{c} = \frac{4\pi j_{z2}}{c} + \frac{1}{c} \frac{\partial E_z}{\partial t} \quad (20)$$

Or

$$4\pi j_{z2} + \partial_t E_z = -4\pi j'. \quad (21)$$

The non-zero current-density deficit, j' , arises from the fact that charge particles are moving at a speed v_0 that is smaller than the Alfvén-wave speed, and is given by (see §2.1 for a detailed derivation)

$$j'(t, z) = \delta z \partial_z j_{z1} = - \left[\frac{\omega_a \delta z}{c} \right] \frac{ck_x B_y(t, z)}{4\pi}, \quad (22)$$

where $B_y(t, z)$ is given by equation (19),

$$\delta z \approx -\frac{ct}{2\gamma_0^2}, \quad (23)$$

and t is the time elapsed since the AW packet entered the charge starvation region.

The current density due to the e^\pm encountered by the CC-AW, which are accelerated to speed v_\pm is

$$j_{z2} = qn_{2+}v_{2+} - qn_{2-}v_{2-} \equiv j_{2+} + j_{2-} = \sum_{\pm} j_{2\pm}, \quad (24)$$

and the time derivative of this current density is

$$\frac{dj_{z2}}{dt} = \sum_{\pm} q_{\pm} \left[n_{2\pm} \frac{dv_{2\pm}}{dt} + v_{2\pm} \frac{dn_{2\pm}}{dt} \right] \quad (25)$$

$$= \sum_{\pm} \left[\frac{q^2 E_z n_{2\pm}}{m\gamma_{\pm}^3} - j_{2\pm} \frac{\partial v_{2\pm}}{\partial z} \right], \quad (26)$$

where $q_{\pm} \equiv \pm q$, and $dj_{\pm}/dt \equiv \partial_t j_{\pm} + v_{\pm} \partial_z j_{\pm}$. We have made use of particle conservation equation, and the equation of motion of a charge particle under electric field, i.e. $d(\gamma_{\pm} v_{\pm})/dt = q_{\pm} E_z/m$ or $dv_{\pm}/dt = q_{\pm} E_z/(m\gamma_{\pm}^3)$ in arriving at the final expression in equation (26). It follows from equation (26) that

$$\frac{\partial j_{z2}}{\partial t} = \frac{\omega_{p2}^2 E_z}{4\pi\gamma_2^3} - \sum_{\pm} \frac{\partial(v_{2\pm} j_{2\pm})}{\partial z}, \quad (27)$$

where

$$\omega_{p2}^2 \equiv \frac{4\pi q^2 n_2}{m}, \quad \frac{1}{\gamma_2^3} \equiv \sum_{\pm} \frac{n_2^{\pm}}{n_2 \gamma_{2\pm}^3} \quad \& \quad n_2 \equiv n_{2-} + n_{2+}. \quad (28)$$

The second term in the expression for $\partial_t j_{z2}$ vanishes when electrons and positrons have opposite velocities, $v_{2-}(t, z) = -v_{2+}(t, z)$, as one might expect when the electric field reverses direction on a length scale much smaller than the AW wavelength, i.e. $\omega_{p2} \gg \omega_a$; we note that this approximation breaks down when $|v_{2\pm}|/c \gtrsim 10^{-1}$. We will use this approximation in our derivation to obtain insights in the behavior of the system. The equation for j_{z2} reduces to

$$\frac{\partial j_{z2}}{\partial t} = \frac{\omega_{p2}^2 E_z}{4\pi\gamma_2^3} \quad (29)$$

with this approximation. Finally, we take the time derivative, at fixed z , of equation (21) and make use of (29) to arrive at

$$\partial_t^2 E_z + \frac{\omega_{p2}^2 E_z}{\gamma_2^3} \approx -4\pi \partial_t j', \quad (30)$$

where j' is given by equation (22). The oscillator equation for E_z can be solved exactly when $\gamma_2 \approx 1$, and the solution is given by

$$E_z(t, z) \approx A \sin(\omega_{p2} t + \phi) - \frac{4\pi \partial_t j'}{\omega_{p2}^2}, \quad (31)$$

where we have taken $\omega_{p2} \gg \omega_a$. The constant A is determined by the condition that at a fixed z , $E_z(t_0, z) = 0$ at time $t_0 = (z - z_0)/c$ that is when the AW head arrives at that point; where z_0 is the z coordinate at the head of the AW wave at $t = 0$. This gives

$$A = \frac{4\pi \partial_t j'(z, t)|_{t_0}}{\omega_{p2}^2 \sin(\omega_{p2} t_0 + \phi)}, \quad (32)$$

the phase ϕ can be determined by the condition that at time t_0 , at z , $j_{z2} = 0$, and therefore, $\partial_t E_z = -4\pi j'(t_0, z)$ as per equation (21).

The solution obtained above for the electric field (eqs. 31 & 32) is a superposition of free and forced oscillations with frequencies ω_{p2} and ω_a respectively. We see this behavior very clearly in our numerical simulation results presented in Fig. 2. The analytic solution (eq. 31) breaks down when particles encountered by the CC-AW are accelerated to speed $\gtrsim c/10$. The second term in equation (27) we neglected is no longer small in that case, and has to be included in the calculation. Moreover, it is no longer a valid approximation to neglect the action of E_z on the current density associated with charge particles advected by the Alfvén wave packet (j_{z1}), as we did in our calculations above. Our numerical simulations, of course, keep track of all these effects.

The electric field strength, shown at $t = 10T_a$ in Fig. 2, is weaker than given in equation (10) by a factor $\sim \omega_{p2}/\omega_a$; [$T_a \equiv 2\pi/\omega_a$ is the Alfvén wave period]. This is because the fresh plasma encountered by the CC-AW shields the electric field effectively but not completely; the residual field is substantially smaller than the field strength generated by current deficit of the CC-AW system as given in eq. 10.

However, the electric field grows exponentially with time as shown in the lower panel of Fig. 3; E_z at $45T_a$ is larger by a factor ~ 500 than the field at $10T_a$, and exceeds the field strength given by eq. 10. We have tried different sets of initial conditions for B_y than the one given in equation (17), and they all have exponentially growing E_z ; the memory of the initial condition is lost after a few or few-tens of AW periods depending on γ_0 . The exponential amplification of E_z is a result of an instability that is very similar to the well known two-stream instability. The linear stability analysis of the CC-AW system encountering low density plasma is presented below in §3.1.1.

We have performed various checks to ensure that the results of numerical calculations presented in this work are reliable and accurate. Our simulation code conserves the total particle number of each charge sign, and the plasma & displacement current-densities it calculates are consistent with the curl of magnetic field. We also checked for numerical stability and errors by changing the size of the spatial grid scale by a factor of 2–20 and found little change to the final results for the electric field, and particle speeds over a fairly long time baseline of $\sim 10^2 T_a$. Moreover, we cross-checked our numerical solutions with analytic results (eq. 31) for t less than a few T_a and found good agreement. And finally, the rate of exponential increase of E_z on a longer time scale shown in Fig. 3 (lower panel) agrees with the linear instability growth rate calculated in §3.1.1 and presented in Fig. 4.

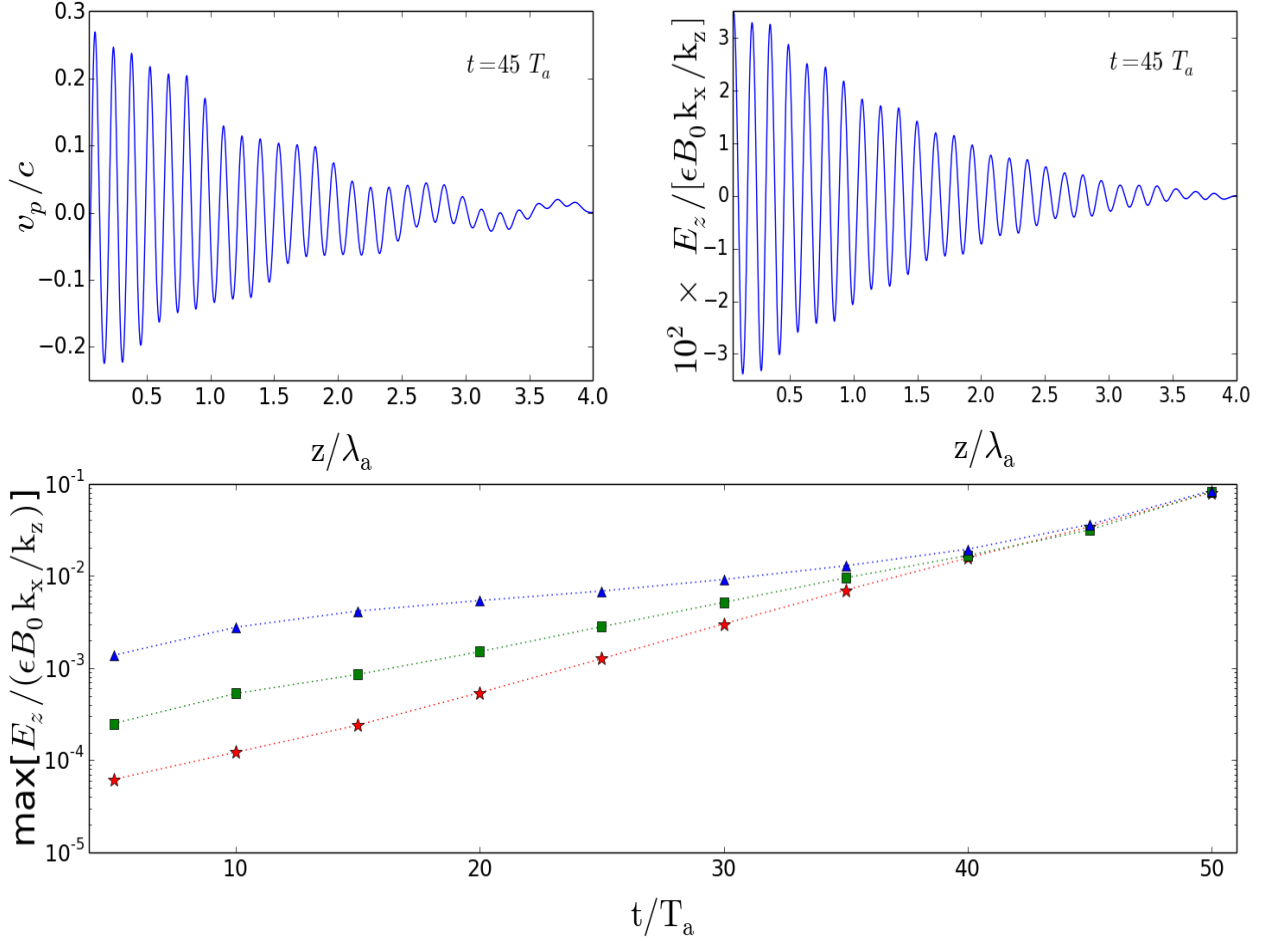


Figure 3. The top left and right panels show v_p and E_z at $t = 45T_a$ – Fig. 2 also showed these variables but at $t = 10T_a$. The parameters for the simulations here are the same as in the calculations presented in Figs. 2, i.e. $\gamma_0 = 10^2$, $k_x/k_z = 0.5$, $\omega_B/\omega_a = qB_0/(mc\omega_a) = 10^5$, $\omega_{p1}/\omega_a = 7.1$ (at the peak of AW), and $\omega_{p2}/\omega_a = 7.1$; see the caption for Fig. 2 for the explanation for what v_p , E_z , T_a , etc. stand for. Note that the electric field E_z at $t = 45T_a$ (top-right) is larger by a factor ~ 200 compared with the field at $t = 10T_a$ (Fig. 2). Furthermore, the data in Fig. 2 clearly shows the superposition of free oscillation at frequency $\omega_{p2} = 7.1\omega_a$ and the forced oscillation at frequency ω_a . The free oscillation grows exponentially with time as described in §3.2, whereas the forced oscillation does not, and the result is that the oscillations of v_p and E_z at $t = 45T_a$ is dominated by frequency ω_{p2} as seen in the upper panels of this figure. The lower panel shows the global maximum of $|E_z(t, z)|/(\epsilon B_0 k_x/k_z)$ – along the finite width of the AW packet at a fixed t – as a function of time for three different values of e^\pm density encountered by the AW packet – the density $n_2/\max(n_{1\pm})$ for the lowest curve (points marked by red-stars) is 0.5, points denoted by green-squares have $n_2/\max(n_{1\pm}) = 0.125$, and for triangles it is 0.031; and all points in this panel are obtained from our numerical simulations of Alfvén wave propagation with initial and boundary conditions specified by equation 17.

3.1.1 A 2-stream like instability associated with CC-AW moving through stationary plasma

The starting point of linear stability analysis is to perturb equation (30), which gives

$$\partial_t^2 E_z + \omega_{p2}^2 E_z = \partial_t \delta [c(\nabla \times B)_z - 4\pi j_{z1}] = -4\pi \partial_t (\delta j_{z1}), \quad (33)$$

when the stationary plasma encountered by the CC-AW are accelerated to speed much less than c . We note that E_z is already a first order perturbation variable, which is non-zero only when $\delta j_{z1} \neq 0$. This is why the perturbation to ω_{p2} does not show up on the left side of the above equation. Moreover, the magnetic field B_y associated with the AW is pre-specified (eq. 19), and its perturbation is taken to be zero in the present analysis.

The equation for current density j_{z1}

$$\partial_t j_{z1} = \frac{q^2 n_1 E_z}{m\gamma_0^3} - \partial_z (v_1 j_{z1}), \quad (34)$$

– which has the same form as eq. 27 – is perturbed to obtain an equation for δj_{z1}

$$\partial_t \delta j_{z1} + v_0 \partial_z (\delta j_{z1}) = \frac{q^2 n_1 E_z}{m\gamma_0^3} - j_{z1} \partial_z \delta v_1 - \delta v_1 \partial_z j_{z1}, \quad (35)$$

where $v_1 = v_0 + \delta v_1$, and v_0 & γ_0 are independent of z as per the initial condition for CC-AW. Both n_1 and j_{z1} are functions of z as given by equation (17), and they oscillate with time with frequency $\omega_a \ll \omega_{p2}$ as follows

$$j_{z1}(z, t) = \epsilon B_0 k_x \cos(\omega_a z/c - \omega_a t), \quad n_1 = \frac{j_{z1}}{qv_0 \text{sign}(j_{z1})}. \quad (36)$$

The equation of motion of a charge particle

$$\frac{dv_1}{dt} = \frac{qE_z}{m\gamma_0^3} \quad (37)$$

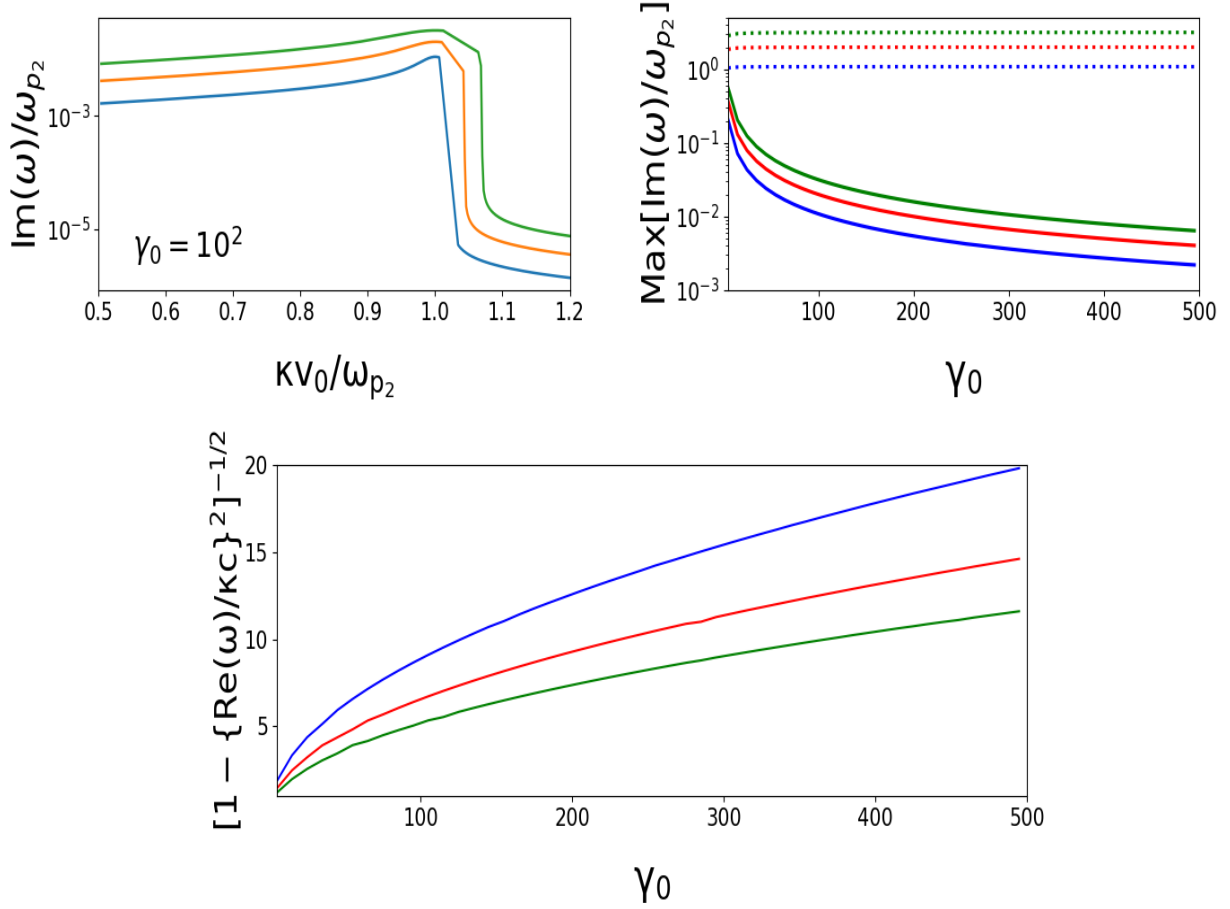


Figure 4. Shown in the top left panel is the growth rate of the instability described in §3.1.1 as a function of wavenumber κ for three different values of ω_{p1}/ω_{p2} , 2 (blue), 5 (red), 10 (green); ω_{p2} , given by eq. 28, is the plasma frequency of the e^\pm -medium encountered by the Alfvén wave packet, ω_{p1} is given by eq. 18, and κ is the wavenumber for the instability. The growth rate of the instability is obtained by solving the dispersion eq. 42 to find the unstable mode. The top right panel shows the growth rate, $-\text{Im}(\omega(k))$, of the fastest growing mode as a function of γ_0 ; γ_0 is the LF of e^\pm -plasma advected by the AW to supply the current density the wave needs, i.e. $c(\nabla \times \mathbf{B}_y)_z/4\pi$. The three different colored curves correspond to different ω_{p1}/ω_{p2} as before. The maximum growth rate scales as $\gamma_0^{-1} \omega_{p1}^{2/3} \omega_{p2}^{1/3}$, as shown by the 3-dotted color curves which are $-\text{Im}(\omega(k)) * \gamma_0$. The bottom panel displays the effective Lorentz factor of the most unstable mode, i.e. $[1 - \{\text{Re}(\omega)/kc\}^2]^{-1/2}$, for the three different values of ω_{p1}/ω_{p2} , viz. 2, 5 & 10.

is perturbed to give

$$\partial_t \delta v_1 + v_0 \partial_z \delta v_1 = \frac{qE_z}{m\gamma_0^3} \quad (38)$$

Taking the t & z dependence of perturbations δv_1 , δj_{z1} and E_z to be $\exp(i\omega t - i\kappa z)$, where κ is the wavenumber of the instability, these equations reduce to

$$i(\omega - v_0\kappa)\delta j_{z1} = \frac{q^2 n_1 E_z}{m\gamma_0^3} + (i\kappa j_{z1} - \partial_z j_{z1})\delta v_1 \quad (39)$$

and

$$i(\omega - v_0\kappa)\delta v_1 = \frac{qE_z}{m\gamma_0^3}. \quad (40)$$

Since n_1 and j_{z1} are functions of time, the above two equations are approximate and only valid when $\text{Re}(\omega) \gg \omega_a$; we show below that $\text{Re}(\omega) \approx \omega_{p2} \gg \omega_a$. Eliminating δv_1 from these two equations we find

$$i(\omega - v_0\kappa)^2 \delta j_{z1} = \frac{q^2 n_1 E_z}{m\gamma_0^3} [\omega + iv_0 \partial_z (\ln j_{z1})], \quad (41)$$

where we used $j_{z1} = qnv_0$.

Substituting this back into equation (33) we obtain the dispersion relation

$$\omega_{p2}^2 - \omega^2 = -\frac{4\pi q^2 n_1 \omega}{m\gamma_0^3} \left[\frac{\omega + iv_0 \partial_z (\ln j_{z1})}{(\omega - v_0\kappa)^2} \right]. \quad (42)$$

One of the four roots of this equation has an imaginary component with negative sign corresponding to exponentially growing solution. The growth rate for a few different parameters are shown in Fig. 4. Numerical solutions of equation (42) show that the growth-rate is highest for

$$\text{Re}(\omega) \approx c\kappa \approx \omega_{p2}, \quad (43)$$

and the dependence of this maximum growth rate on γ_0 , ω_{p1} , and ω_{p2} is (see the top right panel of Fig. 4)

$$\text{Max}[|\text{Im}(\omega)|] \approx \frac{\omega_{p1}^{2/3} \omega_{p2}^{1/3}}{\gamma_0}, \quad (44)$$

Since the instability described in this sub-section is really an over-stable oscillation, i.e. $\text{Re}(\omega) \neq 0$, with finite wavenumber κ . A quantity of interest for later use in this work is the Lorentz factor with

which the oscillations move forward, and that is defined as follows

$$\gamma_{\text{os}} \equiv \frac{1}{\left[1 - \{\text{Re}(\omega)/\kappa c\}^2\right]^{1/2}}. \quad (45)$$

The values of γ_{os} as a function of γ_0 for $\omega_{p1}/\omega_{p2} = 2, 5$ & 10 are shown in the lower panel of Fig. 4. For $\gamma_0 \sim 10$, $\gamma_{\text{os}} \sim 2$, and $\gamma_{\text{os}} \propto \gamma_0^{1/2}$ is a fairly accurate description for how γ_{os} increases for $\gamma_0 \gtrsim 10$ (see Fig. 4).

We close this sub-section by providing a brief discussion of the physical origin of the instability. A key component, or trigger, for the instability is the current density, j_{z1} , associated with charge particles that are being advected by the Alfvén wave. A seed electric field E_z perturbs this current density, δj_{z1} , which in turn has a positive feedback on the electric field. The first term in equation (31) is the important one for the feedback as it causes δj_{z1} to oscillate with frequency ω_{p2} , which then couples to the electric field resonantly. This feedback loop leads to an exponential increase with time of the component of the electric field E_z that oscillates at frequency ω_{p2} , and thus comes to dominate the second term in equation (31) after a few growth times as we see in Fig. 3.

3.2 Charge starved Alfvén wave propagation: solution of exact equations

In the previous sub-section (§3.1), we assumed that the magnetic field perturbation amplitude associated with the Alfvén wave packet (B_y) does not evolve with time as the wave propagates out and an electric field along z develops. This assumption is not strictly correct; it was introduced to simplify analytical calculations and gain physical understanding of the CC-AW system and the emergence of E_z . We drop that assumption in this sub-section and solve, numerically, the exact set of equations (13-14) for the EM field. We keep track of three EM field components, B_y , E_x and E_z , as the CC-AW propagates out and encounters a non-zero density, stationary, plasma. Equations for plasma density evolution and particle dynamics (15) are unchanged. We continue to approximate the system as 1D in space by assuming that the spatial variation in the x direction is given by $\exp(ik_x x)$. This is a good assumption as long as $k_x \ll k_z$ and k_x is not a function of z . The latter is guaranteed to be valid due to the symmetry of the system or the fact that \mathbf{B}_0 is independent of x and thus k_x is a conserved quantity. This can be seen from the following Eikonal equation

$$\frac{dk_i}{dt} = -c \sum_{j=1}^3 k_j \frac{\partial \hat{B}_{0j}}{\partial x_i} \implies \frac{dk_x}{dt} = 0. \quad (46)$$

Results of numerical simulations of the full set of equations are presented in Fig. 5 at $t = 10T_a$ & $45T_a$ for the same set of parameters as in Figs. 2 & 3 except that $ck_x/\omega_{p2} = 0.2$ for calculations in Fig. 5 as opposed to 0.5 in the other two figures. The structure of E_z as a function of z at different times with and without the approximation are similar – both of which show pronounced oscillations at frequency ω_{p2} , which have similar amplitudes to within a factor ~ 2 after we correct for the difference in their respective k_x values; $E_z \propto k_x$ (eq. 13). Moreover, both calculations show a superposition of oscillations of frequencies ω_a and ω_{p2} at early times ($t \lesssim 20T_a$), but later on the exponentially growing mode at frequency ω_{p2} becomes the dominant component.

The growth-rate of E_z with time is shown in the bottom right panel of Fig. 5. The exact calculations find growth-rates that are similar in magnitude to those of the approximate calculations shown

in Fig. 3 after we correct for the factor 2.5 difference in their k_x values. Thus, the instability described in §3.1.1 survives intact for the full set of equations where the magnetic field perturbation, B_y , and the x -component of the electric field (E_x) are accorded full dynamical status and are calculated self-consistently. The results we have presented in these figures are for $\gamma_0 = 10^2$. We have verified numerically that the results for the exact and approximate models are similar for γ_0 between about 10 and 200. One difference we found, however, is that the growth rate, $\text{Im}(\omega)$, declines as γ_0^{-1} when B_y and E_x are pre-set and not allowed to be perturbed, and significantly faster when the dynamics of these fields are included in the calculation self consistently. Our numerical code for the exact solution of eqs. 13–15 is unable to handle $\gamma_0 \gtrsim 200$, and therefore we are unable to quantify the behavior of the instability at larger values of γ_0 . However, according to the approximate analytical calculation of the growth rate presented in §3.1.1 when B_y and E_x are pre-specified, $\text{Im}(\omega)$ is exactly proportional to γ_0^{-1} for all values of γ_0 larger than about 10.

The perturbation to B_y is shown in the lower left panel of Fig. 5. This perturbation, δB_y , is defined to be the difference between the exact numerical solution $B_y(t, z)$ of eqs. 13–15 and the approximate analytic solution given by equation (19). The magnitude of δB_y is similar to E_z (compare the top right and bottom left panels of fig. 5) modulo the factor of k_x for E_z . This means that $k_x \delta B_y$ is much smaller than the $\partial_t E_z \sim \omega_{p2} E_z$ term in the second part of eq. (13) when $ck_x \ll \omega_{p2}$, and that is the reason that the results we obtained when we neglected δB_y did not make a large qualitative difference to the final result for E_z . The value of ck_x/ω_{p2} for our numerical calculations is ~ 0.05 whereas for Alfvén waves in NS magnetosphere the expected value is $\sim 10^{-5}$. Our numerical code cannot handle $ck_x/\omega_{p2} \lesssim 10^{-2}$, but based on the physics of the system we expect the growth-rate of E_z presented in this work to apply to parameters appropriate for NS magnetospheres. We note that the electric field perturbation δE_x is almost identical to δB_y , which is what one expects from the first part of eq. (13).

4 RADIATION FROM THE COHERENT CURRENT OSCILLATING AT PLASMA FREQUENCY

The oscillating current associated with the instability described in §3.1.1, see Fig. 6, produces coherent radiation. The starting point of the calculation of the emergent luminosity is the following exact wave equation

$$\nabla^2 \mathbf{B} - \frac{1}{c^2} \nabla_t^2 \mathbf{B} = -\frac{4\pi}{c} \nabla \times \mathbf{j} \equiv -4\pi \mathbf{S}, \quad (47)$$

where \mathbf{j} is the current density induced by the instability, and \mathbf{S} is the source for EM waves generated by the oscillating current density. The solution of this equation is

$$\begin{aligned} \mathbf{B}(\mathbf{r}, t) &= - \int d^3 r_1 \frac{\mathbf{S}(\mathbf{r}_1, t - |\mathbf{r} - \mathbf{r}_1|/c)}{|\mathbf{r} - \mathbf{r}_1|} \\ &= -\frac{1}{c} \nabla \times \int d^3 r_1 \frac{\mathbf{j}(\mathbf{r}_1, t - r/c + \hat{\mathbf{n}} \cdot \mathbf{r}_1/c)}{r} \end{aligned} \quad (48)$$

where \mathbf{r} is the location at which the field is measured, \mathbf{r}_1 is the location of the oscillating charge at the retarded time $t_1 = t - r/c + (\hat{\mathbf{n}} \cdot \mathbf{r}_1)/c$, and $\hat{\mathbf{n}} \equiv (\mathbf{r} - \mathbf{r}_1)/|\mathbf{r} - \mathbf{r}_1|$ is the unit vector that points from the latter to the former location. As usual, the expansion $|\mathbf{r} - \mathbf{r}_1| \approx r - \hat{\mathbf{n}} \cdot \mathbf{r}_1$ far away from the source ($r \gg r_1$) has been used.

The current density oscillates along the wave propagation direction (z) at a plasma frequency ω_p (Fig. 6), but with amplitude that varies

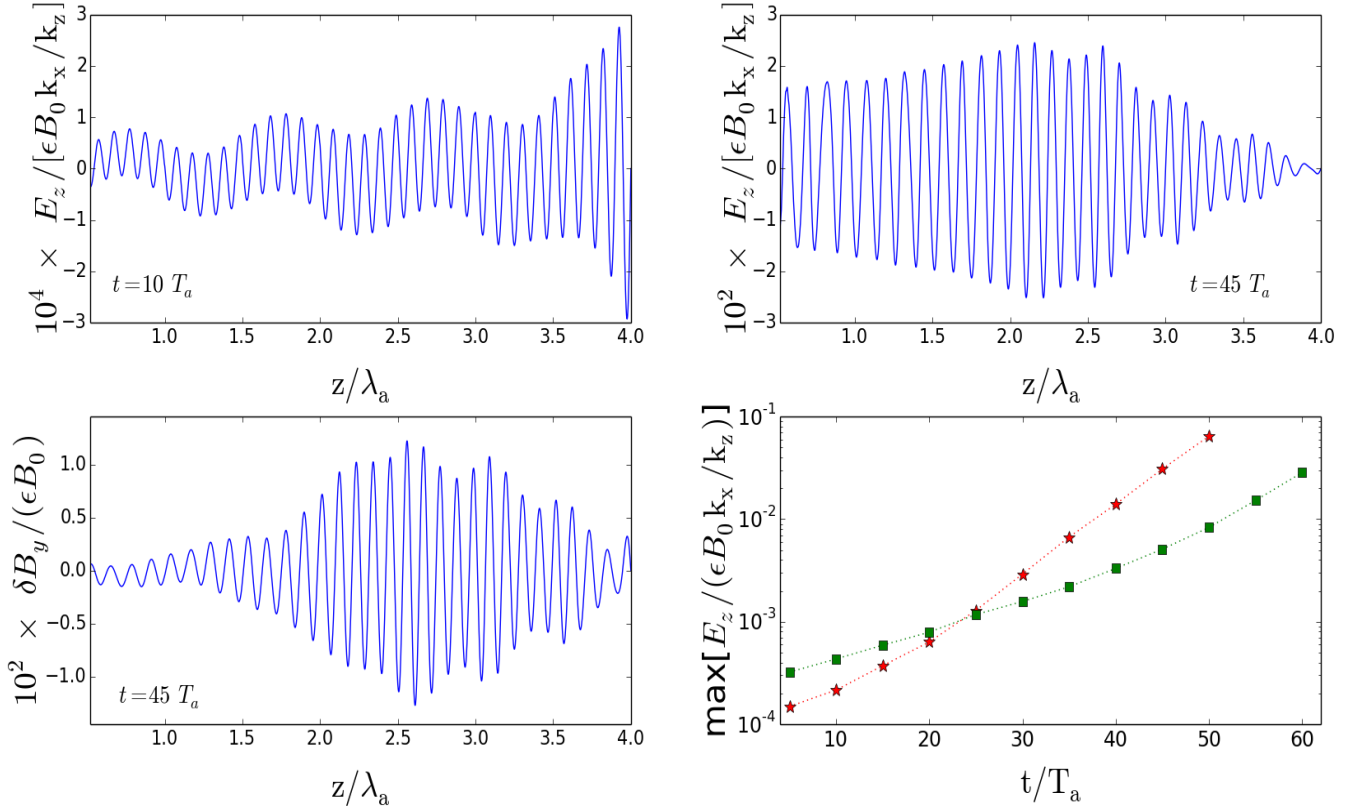


Figure 5. Shown in the top left and right panels are the electric field strength divided by the Alfvén wave amplitude, $E_z/(\epsilon B_0)$, at times $10T_a$ and $45T_a$ respectively and for $k_x/k_z = 0.2$ – the other parameters are the same as in the calculations presented in Figs. 2 & 3, i.e. $\gamma_0 = 10^2$, $\omega_B/\omega_a = qB_0/(mc\omega_a) = 10^5$, $\omega_{p2}/\omega_a = 7.1$; $T_a = 2\pi/\omega_a$ & $\lambda_a = cT_a$ are Alfvén wave period and wavelength respectively. Simulation results presented in this figure were calculated using the full set of equations 13–16 without any simplifying assumption. These results should be contrasted with results in Figs. 2 & 3 where the magnetic field perturbation (B_y) and the x-component of electric field perturbation associated with the AW packet (E_x) were prescribed for all z & t and not calculated self-consistently as is done here. The perturbation to Alfvén wave amplitude, δB_y , – which is the deviation of the y-component of the magnetic field from the expression given in eq. 19 – is shown in the lower left panel. The magnitude of δB_y is of the same order as E_z (top right panel), and is identical to δE_x . The lower right panel shows the peak value of $E_z/(\epsilon B_0)$ as a function of time for two different values of e^\pm plasma density encountered by the AW – the density $n_2/\max(n_1)$ for the points marked by red-stars is 0.5, whereas the density ratio is 0.125 for points denoted by green-squares; where n_1 is given by eq. 17, and all points in this panel were calculated using numerical simulations of Alfvén wave propagation without any approximation. The growth rates of the instability we find here have roughly the same magnitudes as in Fig. 3.

along z . It varies along the other two directions on a much longer length scale of $\sim k_x^{-1}$. Let us write the functional form of \mathbf{j} as

$$\mathbf{j}(\mathbf{r}_1, t_1) = j_0 \hat{\mathbf{z}} \xi(x_1, y_1) \exp(ik_p \eta - \eta^2/\ell_0^2), \quad \eta \equiv z_1 - vt_1, \quad (49)$$

where v is the pattern speed of the oscillating current. Substituting this in equation (48) we find

$$\mathbf{B}(\mathbf{r}, t) = \frac{ij_0 k \hat{\mathbf{z}} \times \hat{\mathbf{r}} \exp(-i\omega t + ikr)}{cr} \int dx_1 dy_1 \xi(x_1, y_1) \times \int dz_1 \exp\left[ik_p z_1 - ik \hat{\mathbf{n}} \cdot \mathbf{r}_1 - (z_1 - \beta \hat{\mathbf{n}} \cdot \mathbf{r}_1)^2/\ell_0^2\right] \quad (50)$$

where $k = \beta k_p$ and $\beta = v/c$. Taking $\hat{\mathbf{n}} = \hat{\mathbf{x}} \sin \theta_0 + \hat{\mathbf{z}} \cos \theta_0$, without loss of generality, and using the small θ_0 and large γ approximations, so that $(1 - \beta \cos \theta_0) \approx (1 + \gamma^2 \theta_0^2)/2\gamma^2$, results in

$$\mathbf{B}_\perp(\mathbf{r}, t) = \mathbf{A}_B \int dx_1 dy_1 \xi(x_1, y_1) \exp(-ikx_1 \theta_0) \times \int dz_1 \exp\left[-\left\{\frac{z_1(1 + \theta_0^2 \gamma^2)}{2\gamma^2 \ell_0} - \frac{\beta x_1 \theta_0}{\ell_0}\right\}^2 + \frac{ik_p z_1(1 + \theta_0^2 \gamma^2)}{2\gamma^2}\right], \quad (51)$$

where $\mathbf{A}_B = (\hat{\mathbf{z}} \times \hat{\mathbf{r}}) k j_0 \exp(-i\omega t + ikr)/cr$ and $\gamma = (1 - \beta^2)^{-1/2}$. It is convenient to rescale, $z'_1 = z_1(1 + \theta_0^2 \gamma^2)/2\gamma^2$, and shift the z'_1 integral range by $\beta x_1 \theta_0$ to simplify the above expression:

$$B_\perp(r, t) = \frac{2\gamma^2 A_B}{1 + \gamma^2 \theta_0^2} \int dx_1 dy_1 \xi(x_1, y_1) \int dz'_1 \exp\left[-\frac{z'^2_1}{\ell_0^2} + ik_p z'_1\right], \quad (52)$$

If the domain of z'_1 integration were to be $[-\infty, \infty]$, then

$$B_\perp(r, t) = \frac{2\pi^{1/2} \gamma^2 A_B \ell_0 \exp(-k_p^2 \ell_0^2/4)}{1 + \gamma^2 \theta_0^2} \int dx_1 dy_1 \xi(x_1, y_1) \quad (53)$$

Let us take $\ell_{\perp \text{coh}}$ to be the smaller of the transverse wavelength of the AW and the size of the transverse coherent emission region. The amplitude of the wave magnetic field then is

$$B_\perp(r, t) \approx \frac{2\pi^{1/2} \gamma^2 k j_0 \ell_0 \ell_{\perp \text{coh}}^2 \exp(-k_p^2 \ell_0^2/4)}{(1 + \gamma^2 \theta_0^2) rc}, \quad (54)$$

and the luminosity when $\lambda/\ell_{\perp\text{coh}} < \gamma^{-1}$ and $\gamma\theta_0 \approx 1$ is

$$L = r^2 B_{\perp}^2 c \approx \frac{\pi \gamma^4 k^2 j_0^2 \ell_{\perp\text{coh}}^4 \exp(-k^2 \ell_0^2/2)}{c}, \quad (55)$$

where for $\gamma \gg 1$, $\beta \sim 1$ and $k_p \approx k$. The exponential suppression factors in equations 51 & 55 are there only when the length of the oscillating current is $\gg \ell_0 \gamma^2$ and its temporal and spacial structure is sinusoidal. Otherwise, the luminosity is much larger than given by eq. 55. The luminosity in (55) is the isotropic equivalent in the observer frame except for the cosmological redshift factors, and it is beamed within an angle $\min\{\gamma^{-1}, \lambda/\ell_{\perp\text{coh}}\}$; $\lambda = 2\pi/k$ is the wavelength of the observed radiation.

For a Gaussian envelope of the sinusoidally oscillating current density with $\ell_0 \gg k^{-1}$, the exponential suppression factor in equation (55) makes the radiative loss too small to be of any practical importance. The current density during the linear growth phase of the instability has the sinusoidal shape with amplitude that varies over a few λ_a as shown in Fig. 6, and therefore radiative losses are small during this period.

As the instability grows and enters the non-linear regime, i.e. when the e^{\pm} speed becomes close to c , the current density fluctuations increase rapidly in space and time, and radiative losses are not small any more. The current density in a segment of plasma of length $\sim k_p^{-1}$ decoheres after the plasma has traveled a distance of order $\ell_{dc} \sim \gamma^2 k_p^{-1}$. This is expected from causality as the length in the frame moving with the pattern speed is larger by a factor γ and the elapsed time in this frame is smaller than the NS rest frame also by a factor γ ; this result is also supported by our simulations. In this regime, radiation from different regions of size ℓ_{dc} can be added incoherently³, and the resulting luminosity from the length of the Alfvén wave packet where the instability has entered the nonlinear phase (z_{cs}), is z_{cs}/ℓ_{dc} times⁴ the luminosity given by equation (55) with $k\ell_0 \sim 1$.

$$L \sim \frac{\gamma^4 j_0^2 \ell_{\perp\text{coh}}^4 z_{cs}}{\ell_{dc} c} \sim \frac{\gamma^2 j_0^2 \ell_{\perp\text{coh}}^4 k z_{cs}}{c} \quad (56)$$

If the transverse size of the region which contributes to the observed radiation is $\ell_{\perp} > \ell_{\perp\text{coh}}$, then the above expression for luminosity should be multiplied with a factor $(\ell_{\perp}/\ell_{\perp\text{coh}})^2$.

The particle density for plasma frequency $\sim 10^9 \text{Hz}$ is $n_e \sim 10^{10} \text{cm}^{-3}$. The current density associated with the instability, during the non-linear phase, is $j_0 \sim qn_e c \sim 2 \times 10^{11} \text{cgs}$. For $\ell_{\perp\text{coh}} \sim 10^4 \text{cm}$, $\gamma \sim 10$, and $z_{cs} \sim 10^8 \text{cm}$, the emergent isotropic equivalent luminosity, due to the fluctuating current associated with the instability is $\sim 10^{38} \text{erg s}^{-1}$, and for $\omega_p/2\pi \sim 10 \text{GHz}$, $L \sim 10^{42} \text{erg s}^{-1}$. The radiation is beamed in a narrow cone of angle $\lambda/\ell_{\perp} \sim 3 \times 10^{-3} \text{rad}$, and its frequency is of order $0.1\omega_p$ as the 2-stream instability growth rate peaks at a wave number $\sim 0.1k_p$.

The rate of loss of energy per particle due to this radiation is $p_r \sim L(\lambda/\ell_{\perp\text{coh}})^2 \gamma^{-2} / [n_e e^2 \ell_{\perp\text{coh}}^2 z_{cs}] \sim m_e c^2 \omega_p$; the factor γ^{-2} in the expression for p_r takes into account that the radiation emitted

³ For a purely sinusoidal envelope, of extent much larger than γ^2/k , the bandwidth of the emergent frequency is very narrow.

⁴ To see that the luminosity is larger by a factor z_{cs}/ℓ_{dc} instead of $z_{cs}k_p$ it is best to go back to eq. (51). When the phase term in the exponent of that integrand is coherent over length scale $\gamma^2 k_p^{-1}$ – which is the distance traveled by the wave when the signal from one end of a region of size k_p^{-1} travels to the other end – the contribution to the integral from that is $A_B \gamma^2 k_p^{-1} \ell_{\perp\text{coh}}^2$. Adding different segments of length $\gamma^2 k_p^{-1}$ incoherently gives the radiated power to scale as $(cr^2)(A_B \gamma^2 k_p^{-1})^2 [z_{cs}/(\gamma^2 k_p^{-1})]$.

in NS rest frame in time interval δt arrives at the observer over a smaller time duration of $\delta t/\gamma^2$. Thus, the radiative loss time is $\sim \omega_p^{-1}$ when particles are not accelerated to highly relativistic speed by the instability.

The shortest growth time for the instability is of order ω_p^{-1} when the relative speed of counter-streaming particles is mildly relativistic (Fig. 4). As discussed before, the radiative loss time is much larger than the plasma time during the linear growth phase of the instability (due to the exponential suppression factor in eq. 55), and therefore the instability grows rapidly on the plasma timescale. When the speed of e^{\pm} approaches c and the plasma becomes turbulent, and radiative losses increase dramatically as given by eq. (56), and the instability saturates at that point.

This result can be rephrased in the following way. The EM radiation comes from plasma modes moving at the pattern speed with Lorentz factor γ (which is of order $\gamma_0^{1/2}$). As long as the rate at which energy is being pumped into these modes is faster than that being radiated away, the modes continue to grow. The total energy density contained in the modes is $E_z^2/(4\pi)$, which can be shown to be $\sim nm c^2$. When E_z reaches the strength such that the non-linearity parameter $E_z q/(m\omega_p c) \sim 1$, radiative losses become of order the energy pumped into the modes by the instability and further growth of plasma mode amplitudes is terminated.

5 INTERACTION OF CHARGE STARVED ALFVÉN WAVES MOVING IN OPPOSITE DIRECTIONS

Alfvén waves moving in opposite directions along a magnetic field line is a likely scenario when the neutron star magnetosphere is shook up by a crustal disturbance. This is because magnetic field perturbations are launched at the surface of the NS where these field lines are anchored. These perturbations travel along the field lines away from the NS and they collide and interact somewhere in the magnetosphere. The interaction is particularly complex, and interesting, when it takes place in the charge starvation region for these Alfvén waves and when the polarization angles of the counter-streaming Alfvén waves are different.

The basic picture that is being suggested is that when Alfvén waves are launched at opposite ends of a magnetic field bundle anchored on NS surface, these waves collide at some height above the NS surface. There are two possibilities to consider for the interaction between these Alfvén waves moving in opposite directions. One of which is where the plasma density is marginally above the critical value for charge starvation everywhere along the wave trajectory when one considers the Alfvén packet traveling from one end of the magnetic bundle to the other and ignore the wave packet coming from the other end of the magnetic bundle. However, the plasma density along the trajectory is insufficient to support the superposition of these two waves. Therefore, the system becomes charge starved in the region where these two waves collide, and it is unavoidable that a strong electric field parallel to the static magnetic field will develop rapidly and with strength of order the Alfvén wave amplitude. Since the plasma density is sub-critical for the combined Alfvén waves moving in opposite directions, they cannot advect charge particles with them to prevent charge starvation. This is because charge particles advected by the wave from a patch in the collision region would create a higher charge deficit there. The strong electric field in the collision region would accelerate charge particles, and under the right conditions they would generate coherent EM emission (Kumar et al. 2017; Kumar & Bošnjak 2020; Lu et al. 2020; Zhang 2020).

The other possibility for the interaction between the counter-

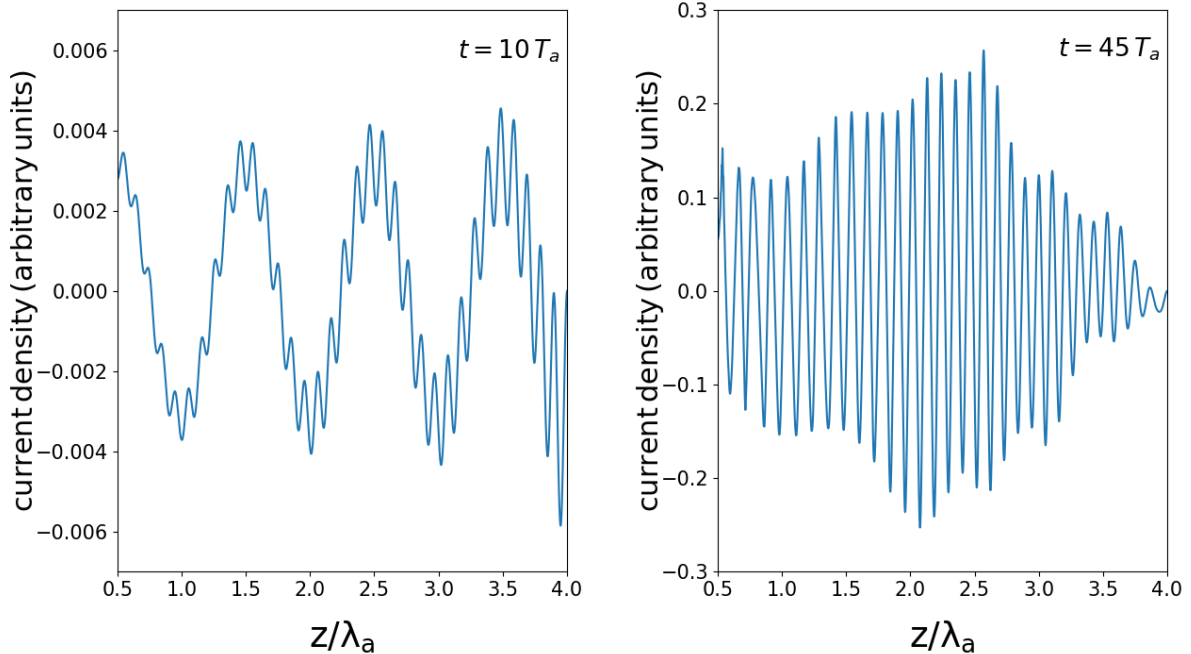


Figure 6. Shown are current densities, $j \equiv q(n^+v^+ - n^-v^-)$, at times $10T_a$ (left panel) and $45T_a$ (right panel). The parameters for these calculations are the same as in Fig. 5. Simulation results presented in this figure were calculated using the full set of equations 13–16 without any simplifying assumption. The current density at $t = 10T_a$, when the perturbation is linear, is sum of two sinusoidal functions of frequencies ω_a and ω_p (Alfvén wave and plasma frequencies respectively). At $45T_a$, the perturbations are mildly nonlinear with particle velocity $\sim 0.3c$, and the current density has fluctuations on roughly the plasma length scale c/ω_p^{-1} .

moving Alfvén waves is that at least one of them has become charge starved at some height before running into the other wave. In this case, the “charge starved” wave is likely to advect charge particles with it as it travel further away from the NS. The CC-AW develops particle density fluctuation and electric field parallel to the magnetic field that also fluctuates on the plasma length scale (§3). When the CC-AWs moving in opposite directions along the magnetic field bundle collide, strong two stream instability leads to formation of particle clumps and development of strong electric field parallel to the unperturbed magnetic field, and likely generation of strong coherent radiation. A discussion of the detailed physics of this interaction is outside the scope of this work.

6 DISCUSSION AND CONCLUSION

An Alfvén wave packet that travels through a medium of ever decreasing plasma density will eventually become charge starved, i.e. it will find itself in a region where the charge density is too small to be able to supply the current needed by the wave even when particles are accelerated to the speed of light. The transition region where particles are rapidly accelerated and carried with the Alfvén wave is not explored in this work. We assumed, instead, that after crossing this transition region, the wave advects just the sufficient number of particles with it, which move with Lorentz factor $\gamma_0 \gg 1$, to avoid charge starvation at larger radii. We have analyzed how the system of charge particles carried with the Alfvén wave (CC-AW) interacts with plasma of finite density it encounters beyond the transition region, and the evolution of the system. The main result we find is that this interaction leads to an instability which is similar to the well known 2-stream instability. Particles advected by the AW, as well as

those encountered by the CC-AW beyond the transition region, form clumps as a result of the instability, and a strong electric field along the direction of the unperturbed magnetic field (E_z) develops⁵. The characteristic wavelength and growth time of the instability are the plasma length and frequency of the stationary plasma encountered by the CC-AW. The spatial scale for the instability is much smaller than the Alfvén-wave wavelength (λ_a) by a factor $\gtrsim 10^4$ in neutron star magnetosphere, and thus according to our numerical simulations strong E_z of order a few percent of AW amplitude develops after the CC-AW has traveled a distance of a few 10s of λ_a .

The scenario we have analyzed in this work (CC-AW) is plausible under some physical situation depending on how the AW makes a transition to the sub-critical density medium; this scenario, where the AW picks up and transports charge particles with it at high LF, is suggested by the work of [Chen et al. \(2020\)](#). One of the main findings of this work is that development of strong E_z even in this scenario where the AW is never truly charge-starved is unavoidable and therefore coherent radio emission should be generated. There is another possible scenario where plasma in the transition zone becomes clumped due to two-stream instability and a strong and oscillating electric field develops that accelerates these clumps to high speed. This too leads to coherent radio waves. We close the paper with a brief discussion of this possibility.

⁵ [Chen et al. \(2020\)](#) reported evidence for a weak 2-stream instability in their PIC simulations. This was likely due to the fact that they considered the Alfvén wave after picking up charges to be moving into very low density medium – almost vacuum, relatively speaking – so that the growth rate of the instability was weak. Furthermore, they followed the Alfvén wave propagation for only a few AW wavelength, and that is too short a time to see the development of a strong electric field and particle clump formation we find.

Electrons and positrons in the transition zone have speed close to that of light. The counter-streaming e^\pm that supply the current to the AW are subject to the 2-stream instability. Even before the onset of the charge starvation, an electric field E_z , along the unperturbed magnetic field \mathbf{B}_0 , develops on spatial scales of $c\omega_p^{-1}$ due to this instability; ω_p is the plasma frequency in the transition zone where the AW is starting to become charge starved. The strength of the field is of order $E_z \sim \delta j/\omega_p \sim \eta c B_y k_x/(4\pi\omega_p)$; where B_y is the Alfvén wave amplitude, and $\eta \equiv [1 - |(4\pi j/c)/(B_y k_x)|]$ is the dimensionless plasma current deficit. This electric field propagates outward like a traveling wave, as discussed in §3.1.1, and therefore particles moving in the same direction as the electric-wave are accelerated for a time, T_E , that is longer than ω_p^{-1} by a factor that depends on the LF of the electric-wave front which is of order a few as shown in Fig. 4. Thus, $T_E \sim 10\omega_p^{-1}$, and particle LF $\gamma_0 \sim 10\omega_p^{-1}qE_z/(mc) \sim \eta\epsilon\omega_B\omega_a/\omega_p^2$; where $\epsilon \equiv B_y/B_0 \sim 10^{-3}$ is the dimensionless Alfvén wave amplitude, and $\omega_B \equiv qB_0/(mc) \sim 3 \times 10^{19} \text{ rad s}^{-1}$ is the cyclotron frequency for magnetars at $\sim 10R_{ns}$. Taking AW frequency $\nu_a \sim 10^4 \text{ Hz}$ and $\nu_p \sim 10^9 \text{ Hz}$, we find $\gamma_0 \sim 10^2$ when the charge deficit η is of order unity. The clumps of particles moving along curved magnetic field lines would produce coherent emission which would also limit their LF to $\sim 10^2$. These clumps would last for at least the light-crossing time in the comoving frame of the clump and that is sufficient for the generation of coherent radiation.

ACKNOWLEDGMENTS

This work has been funded in part by an NSF grant AST-2009619. WL was supported by the Lyman Spitzer, Jr. Fellowship at Princeton University. Some of the work presented here was carried out while PK was visiting the Yukawa Institute (YITP), Kyoto. He is grateful to Prof. Kunihiro Ioka for the hospitality, for organizing an FRB workshop during that visit, and for many stimulating science discussions. He would like to thank YITP for the financial support provided under the Visitors' Program of FY2022, and YITP-W-22-18 for funds for the workshop.

DATA AVAILABILITY

The code developed to perform calculations in this paper is available upon request.

REFERENCES

- Chen A. Y., Yuan Y., Beloborodov A. M., Li X., 2020, arXiv e-prints, p. [arXiv:2010.15619](https://arxiv.org/abs/2010.15619)
- Cooper A. J., Wijers R. A. M. J., 2021, *MNRAS*, **508**, L32
- Ioka K., Zhang B., 2020, *ApJ*, **893**, L26
- Krall N. A., Trivelpiece A. W., 1973, Principles of plasma physics. McGraw-Hill Kogakusha
- Kulsrud R. M., 2005, Plasma physics for astrophysics. Princeton University Press
- Kumar P., Bošnjak Ž., 2020, *MNRAS*, **494**, 2385
- Kumar P., Lu W., Bhattacharya M., 2017, *MNRAS*, **468**, 2726
- Lu W., Kumar P., 2018, *ApJ*, **865**, 128
- Lu W., Kumar P., Zhang B., 2020, *MNRAS*, **498**, 1397
- Qu Y., Zhang B., 2021, arXiv e-prints, p. [arXiv:2111.12269](https://arxiv.org/abs/2111.12269)
- Wang W.-Y., Yang Y.-P., Niu C.-H., Xu R., Zhang B., 2021, arXiv e-prints, p. [arXiv:2111.11841](https://arxiv.org/abs/2111.11841)
- Yang Y.-P., Zhang B., 2018, *ApJ*, **868**, 31
- Zhang B., 2020, *Nature*, **587**, 45